Real-time monitoring of steady-state pulsed chemical beam epitaxy by p-polarized reflectance

K.J. Bachmann[a,b,c,*], N. Sukidi[a], C. Höpfner[a], C. Harris[a], N. Dietz[a,d], H.T. Tran[c], S. Beeler[c], K. Ito[c], H.T. Banks[c]

[a] *Department of Materials Science and Engineering, North Carolina State University, Raleigh, NC 27695, USA*
[b] *Department of Chemical Engineering, North Corolina State University, Raleigh, NC 27695, USA*
[c] *Center for Research in Scientific Computation, North Carolina State University, Raleigh, NC 27695, USA*
[d] *Department of Physics, North Carolina State University, Raleigh, NC 27695, USA*

Abstract

The structure in the p-polarized reflectance (PR) intensity $R_{p4}(t)$ – observed under conditions of pulsed chemical beam epitaxy (PCBE) – is modeled on the basis of the four-layer stack: ambient/surface reaction layer (SRL)/epilayer/substrate. Linearization of the PR intensity with regard to the phase factor associated with the SRL results in a good approximation that can be expressed as $R_{p4} = R_{p3} + \Delta R_p$. R_{p3} is the reflectivity of the three-layer stack ambient–epilayer–substrate. ΔR_p describes the properties of the SRL. An explicit relation is derived between $\Delta R_p(t)$ and the time-dependent surface concentrations $c_h(t)$ ($h = 1, 2, \ldots, N$) of the constituents of the SRL, which holds for conditions of submonolayer coverage of the surface by source vapor molecules. Under conditions of low temperature PCBE at high flux, the SRL is expected to exhibit nonideal behavior, mandating replacement of the surface concentrations by activities. Also, in this case, the thickness of the SRL must be represented in terms of partial molar volumina V_h. Since the relation between $\Delta R_p(t)$ and the activities of reactants, intermediates and products of the chemical reactions driving heteroepitaxial growth is non-linear, the extraction of kinetic parameters from the measured time dependence of the PR signal generally requires numerical modeling. © 1998 Published by Elsevier Science B.V. All rights reserved.

Keywords: p-Polarized reflectance; Surface kinetics; Chemical beam epitaxy; Real-time process monitoring

1. Introduction

We have explored p-polarized reflectance spectroscopy (PRS) in the context of real-time monitoring of pulsed chemical beam epitaxy (PCBE) [1–5]. PRS provides high sensitivity to changes in the mix of

---

* Corresponding author. Present address: Department of Materials Science and Engineering, North Carolina State University, Rayleigh, NC 27695, USA. Fax: + 1 919 575 3419; e-mail: bachmann@mte.ncsu.edu.

reactants, intermediates and products of chemical reactions on the surface of the epitaxial film that drive the crystal growth process. Optical monitoring at resonant frequency of a specific reactant or product of the rate limiting reaction preceding growth may enable forward-looking process control that places the detection of deviations of the actual from the desired process evolution ahead of the growth step. Thus corrections in surface chemistry may be possible before locking errors in composition into the developing heteroepitaxial structure. As a prerequisite for work on this topic the surface kinetics must be understood in more detail than presently available, and the measured p-polarized reflectivity R_p must be related to surface composition. In this paper we present explicit relations between the measured time-dependent PRS intensity and surface composition. Where needed, illustrative examples are provided of GaP chemical beam epitaxy on Si(1 0 0) utilizing triethylgallium (TEG) and tertiary-butylphosphine (TBP) as source vapors.

The thermal decomposition of TBP has been thoroughly investigated [6–8] and proceeds through a series of consecutive reactions, e.g.,

$$C_4H_9PH_2 \rightarrow |PH_2^{\cdot} + C_4H_9^{\cdot}, \tag{1}$$

$$C_4H_9^{\cdot} + C_4H_9PH_2 \rightarrow C_4H_9\bar{P}H^{\cdot} + C_4H_{10}, \tag{2}$$

$$C_4H_9|\bar{P}H^{\cdot} \rightarrow |\bar{P}H + C_4H_9^{\cdot}. \tag{3}$$

Also, the kinetics of TEG pyrolysis on III–V surfaces has been studied in detail [9–11] and progresses in three consecutive steps:

$$Ga(C_2H_5)_3 \rightarrow Ga(C_2H_5)_2^{\cdot} + C_2H_5^{\cdot}, \tag{4}$$

$$Ga(C_2H_5)_2 \rightarrow |GaC_2H_5 + C_2H_5^{\cdot}, \tag{5}$$

$$|GaC_2H_5 \rightarrow |Ga^{\cdot} + C_2H_5^{\cdot} \tag{6}$$

(dashes and superscript dots referring to lone electron pairs and single valence electrons, respectively). In preceding work focusing on CBE of GaP on Si(1 0 0) using TEG and TBP as source vapors, we have shown that the decomposition of TBP is fast and the decomposition of TEG fragments represents the rate limiting step [3]. Depending on the delay between the TEG and TBP source vapor pulses, carry-over of TEG fragments from one precursor pulse cycle to the next occurs. It establishes in steady-state a surface reaction layer (SRL) on the epitaxial film, consisting of a mixture of reactants and products of the chemical reactions that drive the epitaxial growth process. Efficient growth occurs within limited process windows that extend over the temperature ranges $260°C \leqslant T \leqslant 410°C$ and $260°C \leqslant T \leqslant 450°C$, for Si(1 0 0) and Si(1 1 1), respectively [13]. Near the upper limits of these process windows we expect monoethylgallium (MEG) and gallium ad-atoms to be the primary Ga containing precursors to growth. However, near the lower limits of these process windows the SRL may contain, in addition to TBP fragments, diethylgallium (DEG), MEG and gallium ad-atoms (see Ref. [12] for comparison to TEG decomposition on GaAs(1 0 0)). In either case, the linkage of measured PRS signal and surface kinetics must focus onto the four-layer stack: (1) ambient–(2) SRL–(3) epilayer–(4) substrate, which represents the simplest realistic description of the optical response under the conditions of CBE operating at low temperature. A schematic representation of this model is shown in Fig. 1.

In view of the high polarizability of the molecular fragments the dielectric function of the SRL is expected to be large compared to that of the organometallic source compounds. This is coroborated by the analysis of the PRS signal under the conditions of PCBE for GaP heteroepitaxy on Si [4, 14] (see also Tables 1 and 2). None of the usual group V hydride, alkyl-substituted group V hydride and metalalkyl source compounds used in III–V vapor phase epitaxy are expected to absorb in the visible, i.e. the imaginary part of the dielectric function of the SRL should be negligible within this energy range. However, PRS data for GaP heteroepitaxy on Si(1 0 0) taken at 632.8 nm show that the SRL is clearly absorbing and provides further evidence for the presence of intermediate products in the SRL (see Table 1). Similar results, albeit at shorter wavelength, have
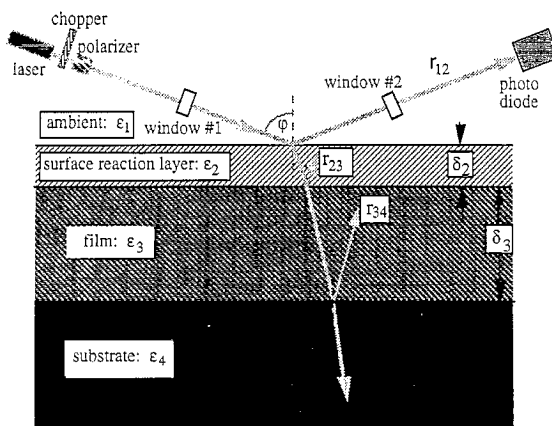
Fig. 1. Schematic representation of p-polarized reflectance on a four-layer stack: ambient/surface reaction layer/epilayer/substrate.

Table 1
Parameters for the modeling of $R_p(t)$ for PCBE of GaP on Si(1 0 0) at $\lambda = 632.8$ nm and $\varphi_1 = 75.64°$

Dielectric functions	Fresnel coefficients
ε_1 (ambient) = 1	$r_{12} = -0.102 + 0.057i$
ε_2 (SRL)[a] = 9.5 + 2.5i	$r_{23} = 0.018 - 0.058i$
ε_3 (GaP) = 10.6	$r_{34} = 0.084 + 0.0026i$
ε_4 (Si) = 15.27 + 0.17i	$r_{13} = -0.084$

[a] The time-averaged value for the dielectric function of the SRL is based on a numerical analysis of the fine structure of Fig. 2 using the time-dependent phase model [23].

Table 2
Representative values of parameters for the modeling of $R_p(t)$ for PCBE of GaP on Si(1 0 0) at $\lambda = 632.8$ nm and $\varphi_1 = 75.64°$ for $0 \leqslant \beta_3 \leqslant \pi$

Parameters	Coefficients
$-0.17 < a_1 < 0.0002$	
$-0.084 < a_2 < 0.084$	$0 < A < 0.084$
$0.99 < b_1 < 1.01$	$-0.059 < B < 0.02$
$-0.007 < b_2 < 0.007$	$-0.052 < C < 0.008$
$-0.066 < a'_1 < 0.012$	
$-0.142 < a'_2 < 0.027$	

been reported for investigations of GaAs growth based on results of surface photoabsorption (SPA) measurements [11]. In conjunction with changes in surface reconstruction and structure of steps associated with changes in surface composition the description of heteroepitaxial growth thus is complex, and is presently far from being understood.

Several supplementing methods of real-time process monitoring must be combined to address this problem (see Ref. [15] for a recent comprehensive review). We have utilized PRS in combination with reflectance difference spectroscopy (RDS), and laser light scattering (LLS) [2]. Recently we have added also simultaneous SPA measurements. Since SPA operates in the strongly absorbing wavelength region, it monitors strictly near surface properties. Thus it supplements PRS, which operates in the weakly absorbing wavelength regime and thus monitors bulk film properties in addition to changes in the chemistry and structure of the surface and film/substrate interface. In the strongly absorbing wavelength region only the surface contributes to the scattering, while at below band gap energy both contributions of surface and interface roughening are observed. Therefore, LLS under conditions of simultaneous SPA and PRS measurements allows separation of surface and interfacial roughening. However, although SPA, PRS and LLS are sensitive to changes in surface structure they are not designed to distinguish between surface chemistry and surface anisotropy. The detection of the latter is the specific strength of RDS. In RDS investigations of III–V epitaxy on (1 0 0) oriented substrates the difference between the reflectivity for light polarized parallel to [0 1 1] and [0 $\bar{1}$ 1] is measured, so that bulk contributions are suppressed and only surface contributions are observed that do not cancel due to reduced symmetry of the reconstructed surface [16]. Similarities exist between RDS and SPA in their surface sensitivity and spectral regions of resonance [17, 18]. However, since RDS probes for anisotropy it senses changes in surface chemistry indirectly as an effect on surface structure. Thus the monolayer oscillations observed in RDS are explained in analogy to the monolayer oscillations in the RHEED intensity under conditions of MBE or CBE as an effect of cyclic island formation and coalescence of islands during the course of monolayer by monolayer growth. Using effective medium theory this has been translated into a cyclic change in the surface dielectric function and anisotropy [19] and has been utilized for control of growth of multiple confined heterostructures [20]. RDS also has been utilized successfully in studies of surface composition. For example, RDS investigations of the changes in anisotropy for the GaAs(1 0 0)c(4 × 4) and Inp(1 0 0)c(2 × 4) surfaces upon exposure to arsine or tertiary-butylarsine (TBAs) are phosphine or TBP, respectively, provide useful information regarding the supply of arsenic and phosphorus to these two surfaces. However, these investigations cannot discern specific bonding configurations on the surface [21]. Since by working close to the pseudo-Brewster angle both SPA and PRS afford high sensitivity to surface chemistry changes even in the absence of anisotropy, in our opinion, they are generally better suited for probing the composition of the SRL than RDS. Both RDS and SPA differ from PRS in that they do not monitor bulk film properties, and thus lack the basis for simultaneous monitoring of instantaneous growth rate and surface kinetics features in the fine-structure for individual source vapor pulse cycles. Of course, under the conditions of PCBE, combinations of spectroscopic ellipsometry (SE) and RDS are equally suitable for simultaneous monitoring of film growth and surface kinetics. However, since depolarization effects are more strongly manifested in measurements of phase than in measurements of amplitude RDS and SE are expected to be less robust with regard to increases in operating pressure than SPA and PRS [22].

2. Relation between reflectance and composition of the SRL

Since the thickness δ_2 of the SRL always remains small compared to the wavelength λ of the light beam at which it is evaluated the complex reflected amplitude r_{p4} of the four-layer stack (1) ambient–(2) SRL–(3) epilayer–(4) substrate can be linearized with regard to the phase factor β_2 associated with the SRL, i.e.,

$$r_{p4} = r_{p4}|_{\beta_2=0} + \left(\frac{\partial r_{p4}}{\partial \beta_2}\bigg|_{\beta_2=0}\right)\beta_2 + \cdots .$$

(7)

As shown in Appendix A, the first term in Eq. (7) is identical to the reflectivity R_{p3} of the three-layer stack ambient–epilayer–substrate. Therefore, the reflectivity of the four layer stack $R_{p4} = r_{p4}r_{p4}^*$ can be represented in the form $R_{p4} = R_{p3} + \Delta R_p$. In the linearized approximation of Eq. (7), ΔR_{p1} is represented by three terms given in Eq. (A.23), which – with assumptions discussed in more detail in Appendix A – can be written as compact simplified representation ΔR_{ps} in terms of the magnitude, real and imaginary parts of $\beta_2 = \beta_{2r} + \beta_{2i}$ as

$$\Delta R_{ps} = A|\beta_2|^2 + B\beta_{2r} + C\beta_{2i}, \tag{8}$$

where A, B, and C are functions of the Fresnel coefficients $r_{k,k+1}$, $k = 1, 2, 3$ for the interfaces ambient/SRL, ambient/epilayer, and SRL/substrate, respectively. Due to interference of partial waves reflected at the surface of the epilayer and the epilayer/substrate interface oscillations are observed in R_{p3} with distance between maxima or minima

$$\Delta \delta_{3m} = \frac{\lambda}{2\sqrt{\varepsilon_3 - \varepsilon_1 \sin \varphi_1}}. \tag{9}$$

In conjunction with a measurement of the time interval t_{i0} associated with the epitaxial growth between adjacent maxima or minima in R_{p3} this permits the determination of an average value for the growth rate $\bar{v}_g = \Delta \delta_{3m}/t_{i0}$. The remaining three terms in Eq. (7) represent a fine structure that is superimposed on the interference oscillations having same periodicity as the source vapor cycle $t_{svc} \ll t_{i0}$.

Fig. 2a shows an example of a typical PRS trace recorded under the conditions of GaP heteroepitaxy on Si(1 0 0). Here the average growth rate is 1.6 Å/s corresponding to an incremental growth of the epilayer by $\overline{\Delta \delta_{3svc}} = 4.8$ Å per source vapor cycle in average, that is, more than two molecular layers of GaP. Since $\overline{\Delta \delta_{3svc}}$ depends weakly on the delay of the TEG pulse after arrival of the TBP pulse, but increases substantially with increasing length of the delay between the TEG pulse and the following TBP pulse, the kinetics of TBP decomposition reaction is fast and the kinetics of the TEG decomposition to fragments enabling crystal growth is slow on the time scale $t_{svc} = 3$ s, which is the duration of the source vapor cycles in this particular experiment (see Fig. 2b). Note that the instantaneous growth rate in the experiment of Fig. 2a is not feedback controlled and fluctuates due to variations in both t_{svc} and the flux of source vapor molecules to the surface. An opportunity to control the instantaneous growth rate associated with each source vapor cycle is given by using the difference between the measured instantaneous slope $\Delta R_{svc}/t_{svc}$ and the theoretically predicted slope $\partial R_{p3}/\partial t$ as control input. As shown in Ref. [14], the precision of monitoring molecular layer epitaxy is typically of the order of 3–5%, depending on the length of time averaging in the acquisition of the PRS signal, i.e., the chosen growth rate.

Fig. 3 shows on the bottom trace the calculated PR intensity at 632.8 nm wavelength for the case of GaP heteroepitaxy on Si using the date given in Table 1. The top trace of Fig. 3 shows the difference between experimental results for R_{p4} and calculated results for R_{p3} based on Eq. (A.10) for growth of GaP on Si. The three traces in between the top and bottom traces reveal the calculated contributions $A|\beta_2|^2$, $B\beta_{2r}$ and $C\beta_{2i}$ to ΔR_{ps}. All three contributions are significant with $B\beta_{2r}$ and $A|\beta_2|^2$ making the largest and smallest contributions, respectively.

The top trace of Fig. 4 shows the relative error $(\Delta R_{ps} - \Delta R_{pex})/\Delta R_{pex}$ for the calculated envelope function, based on the simplified linear approximation Eq. (8) as compared to $\Delta R_{pex} = R_{p4ex} - R_{p3}$ (shown as bottom trace), where R_{p4ex} refers to experimental data and R_{p3} calculated on the basis of Eq. (A.10). The middle trace shows the relative error $(\Delta R_{p1}(t) - \Delta R_{pex})/\Delta R_{pex}$ for the calculated envelope function, based on the linear approximation Eq. (A.5), as compared to ΔR_{pex}. Of course, both errors diverge at the crossing points in the finestructure, where $R_{p4} - R_{p3}$ vanishes [4]. Outside this range the relative error is $< 3\%$ for both $\Delta R_{p1}(t)$ and $\Delta R_{ps}(t)$. Thus, in case of GaP epitaxy of Si, the simplified linear approximation is of comparable validity as the linear approximation, and can be used in a more detailed analysis of the relation of ΔR_{ps} to the chemical reaction kinetics. The sensitivity of the four-layer stack model to changes in parameters describing
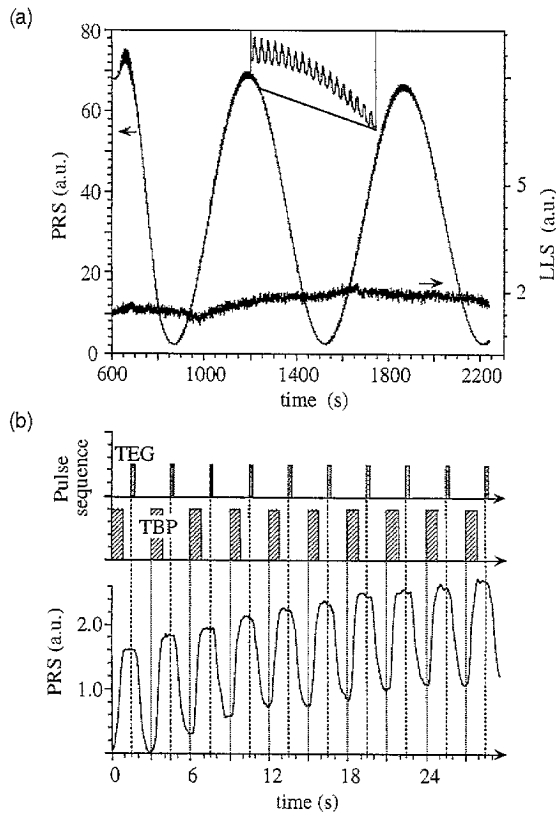
Fig. 2. (a) P-polarized reflectance at 632.8 nm wavelength as a function of time during PCBE of GaP on Si(1 0 0) at 350°C using t-butylphosphine (TBP) and triethylgallium (TEG) as source vapors; inset: magnified view of PR fine structure. (b) Periodic source vapor pulse sequence (top) and associated PR fine structure response (bottom) for the same experiment as shown in Fig. 2a.

the SRL is discussed in detail in Ref. [23]. As shown there, the crossing point positions are invariant to changes in δ_2, but exhibit distinct changes that permit the independent determination of ε_{2r} and ε_{2i} with an accuracy of $\sim 10\%$.

For the interpretation of the time-dependence of R_p in terms of the chemical kinetics in the SRL that drives epitaxial growth in steady-state ε_2 must be linked to the composition of the SRL. As shown in Appendix B, such a linkage is given by

$$\varepsilon_2(\omega) = 1 - \frac{4\pi q^2 N_A}{m} \sum_h c_h F_h(\omega), \tag{10}$$

where N_A is Avogadro's number and

$$c_h = \frac{N_h}{N_A V_m} = \frac{n_h}{V_m} \tag{11}$$

is the molar concentration, i.e., the number of moles n_h of constituent h in volume V_m of the mixture of reactants and products constituting the SRL. The function $F_h(\omega)$ – defined in Appendix B – is an inherent
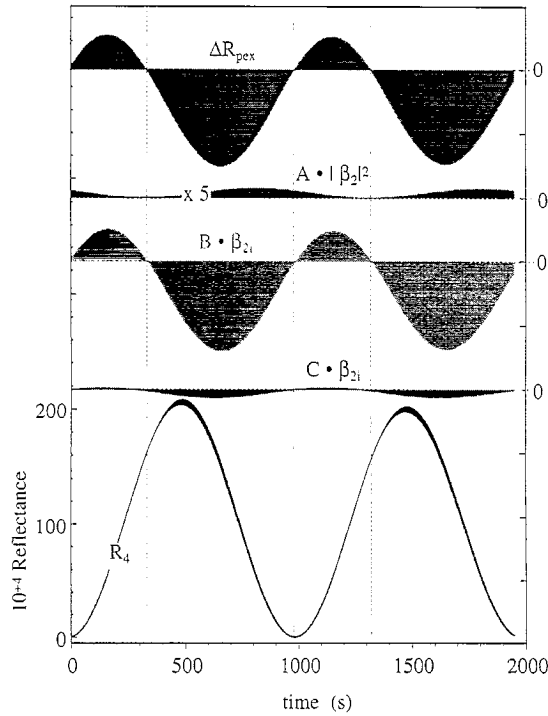
Fig. 3. Calculated PR intensity at 632.8 nm wavelength and $\varphi_1 = 75.64°$ for heteroepitaxy of GaP on Si(1 0 0) based on the time-dependent phase model [23] (bottom trace); experimentally observed fine structure R_{p4exp} minus R_{p3} (top trace) calculated on the basis of Eq. (A.16); calculated contributions $A|\beta_2|^2$, $B\beta_{2r}$ and $C\beta_{2i}$ (traces 2, 3 and 4 from top) to the simplified approximation of the fine structure ΔR_{ps}.

property of each individual constituent. It depends on frequency ω of the incident light beam, but is independent of c_h. At low surface coverage,

$$\Delta R_{ps}(t) = A \frac{4\pi^2 \delta_2(t)^2}{\lambda^2} \frac{\left\{ \left[1 - \frac{4\pi q^2 N_A}{m} \sum_h c_h F_{hr}(\omega) \right]^2 + \left[\frac{4\pi q^2 N_A}{m} \sum_h c_h F_{hi}(\omega) \right]^2 \right\}}{1 - \frac{4\pi q^2 N_A}{m} \sum_h c_h F_{hr}(\omega)}$$

$$+ B \frac{2\pi \delta_2(t)}{\lambda} \left(1 - \frac{4\pi q^2 N_A}{m} \sum_h c_h F_{hr}(\omega) \right)^{1/2}$$

$$+ C \frac{4\pi^2 q^2 \delta_2(t) N_A}{m\lambda} \frac{\sum_h c_h F_{hi}(\omega)}{\left(1 - \frac{4\pi q^2 N_A}{m} \sum_h c_h F_{hr}(\omega) \right)^{1/2}}. \tag{12}$$

Thus even under conditions where the SRL behaves as an ideal solution and $\varepsilon_2(\omega)$ is linear in c_h, R_{p4} is nonlinear. Under conditions of high flux at low processing temperature, where the SRL behaves like
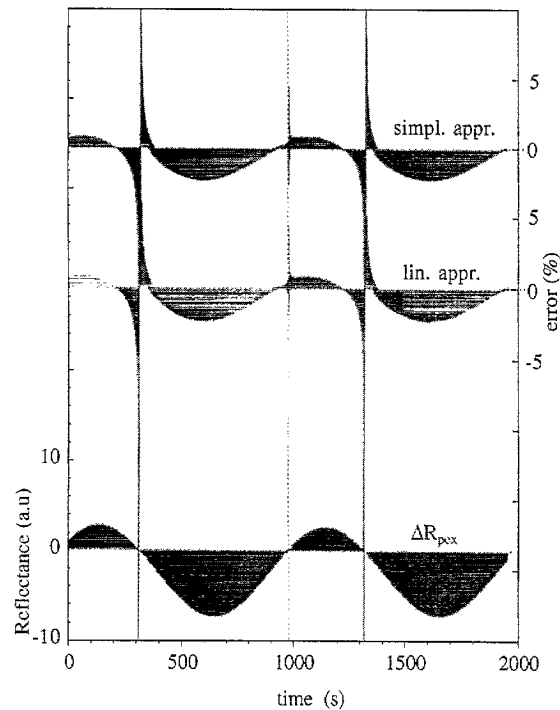
Fig. 4. Comparison of relative errors associated with the approximations of the fine structure by Eqs. (A.14) and (A.18), respectively. Bottom trace: fine structure $\Delta R_{pex} = R_{p4} - R_{p3}$ calculated on the basis of Eqs. (A.1) and (A.16). Middle trace: relative error in the PR intensity $(\Delta R_{pex} - \Delta R_p)/\Delta R_{pex}$ calculated on the basis of Eq. (A.26). Top trace: relative error in the PR intensity $(\Delta R_{pex} - \Delta R_{ps})/\Delta R_{pex}$ calculated on the basis of Eq. (8).

a nonideal solution, a realistic representation of vapor deposition and etching processes must account for modifications of both its dielectric function and the rate constants of the surface chemical reactions by the intermolecular interactions. The correction of the rate constants for reactions in nonideal mixtures is accomplished by incorporation of the activity coefficients of the reactants and products that modify the representation of the activated complex [24]. The definition of the activity coefficient f_h of constituent h in a nonideal mixture is given by the formulation of its chemical potential

$$\mu_h = \mu_{h0} + RT \ln a_h = \mu_{h0} + RT \ln f_h x_h = \mu_h(\text{ideal mixture}) + RT \ln f_h , \tag{13}$$

where $x_h = n_h/\sum_g n_g$ $(g = 1, 2, \ldots, h, \ldots, N)$ is the molar fraction, so that the standard state is defined in the limit $a_h \to 1$. The volume of the nonideal mixture of reactants and products forming the SRL is given by

$$V_m = \sum_h n_h V_h , \tag{14}$$

where $V_h = [\partial V/\partial n_h]_{p,T,ng \neq h}$ $(g = 1, 2, \ldots, N \neq h)$ is the partial molar volume of constituent h. In contrast to local field theory that accounts for dipole–dipole and other intermolecular interactions by a modification of $F_h(\omega)$, we choose to maintain the values of $F_h(\omega)$ for ideal behavior of the SRL, capturing the effects of all interactions of constituent h with other constituents by multiplication of its concentration by f_h. Both

representations of intermolecular interactions cause the same change of the contribution of constituent h to $\varepsilon_2(\omega)$. Then

$$\varepsilon_2(\omega) = 1 - \frac{4\pi q^2 N_A}{m} \sum_h a_h F_h(\omega) = \varepsilon_{2r}(\omega) + i\varepsilon_{2i}(\omega), \tag{15}$$

with

$$a_h = f_h \bar{V} c_h = f_h x_h, \tag{16}$$

where

$$\bar{V} = \frac{V_m}{\sum_h n_h} \tag{17}$$

is the average molar volume. Although the definitions of a_h through Eq. (13) and Eqs. (15) and (16) are closely related, the details of their correlation require further assessment.

Eq. (18) provides the basis for relating the time dependence of ΔR_{ps} to changes of the activities of the constituents of the SRL in time – associated with the chemical reactions that drive the heteroepitaxial growth process. In steady-state, the variations in the supply of source vapor molecules to the SRL are reflected by changes in the activities of all constituents about time-averaged values with same periodicity as the source vapor cycle. Although a commensurate variation of β_2 ensues, the effects of variations in ε_2 on β_2 must be augmented by an assessment of the thickness of the SRL

$$\delta_2(t) = \sum_h \frac{n_h(t) V_h(t)}{A(t)}, \tag{18}$$

where $A(t)$ is the true area of the solid/SRL interface. $A(t)$ changes as the surface of the epitaxial film roughens in the course of epitaxial growth. On the time scale of the source vapor cycle, the changes in $A(t)$ may be negligible. For short periods of growth, $\delta_2(t)$ thus may be expected to follow the periodic variations in the a_h, i.e., to oscillate in steady-state about an average value with the periodicity of the source vapor cycle. The roughening of the SRL/film interface over longer periods of growth is an important aspect of real-time process modeling, and must be monitored by LLS and other supplementing techniques. Under favorable circumstances the variation of $A(t)$ can be kept small (see LLS trace in Fig. 2).

For ε_2 outside the range specified by the above conditions, Eq. (A.1) must be used to achieve accurate results by numerical simulations. Also, during the initial phase of nucleation and coalescence of islands into a contiguous heteroepitaxial layer the above modeling is invalid for the following reasons: (i) local variations of the composition of the SRL due to differences in the reaction kinetics on surface elements of the epitaxial film and yet uncoated surface elements of the substrate; (ii) modifications of the effective dielectric function for a porous film as compared to a contigous film of the same material; (iii) interface broadening, i.e. incorporation of constituents of the substrate into the heteroepitaxial film, which can be a particular problem in the case of polar-on-nonpolar growth. Since the nucleation and coalescence stage of heteroepitaxy determines to a large extent the density and distribution of defects in the epilayer, and thus sets the stage for roughening of the surface and buried interfaces upon subsequent steady-state growth, further work is required to establish a valid description of this important period in the evolution of the heteroepitaxial stack.

3. Summary and conclusions

We have analysed the structure in the PR intensity $R_{p4}(t) = r_p r_p^*$, observed under conditions of pulsed chemical beam epitaxy (PCBE), for the four-layer stack: ambient|SRL|epilayer|substrate. Linearization of

r_p results in an approximation to the reflectance consisting of four terms. One of these terms represents the interference oscillations in the reflectance $R_{p3}(t)$ of the three-layer stack: ambient|epilayer|substrate. The remaining three terms represent the fine structure $\Delta R_p(t)$ that is superimposed onto $R_{p3}(t)$ and is resolved under the conditions of pulsed chemical vapor deposition. An explicit relation is derived between $\Delta R_p(t)$ and the time-dependent surface concentrations c_h ($h = 1, 2, ..., N$) of the constituents of the SRL. Under conditions of low temperature PCBE at high flux, the SRL represents a nonideal condensed phase, requiring replacement of the surface concentrations by activities. Also, the thickness of the SRL must be represented in terms of partial molar voluminea V_h. Since the time dependences of a_h and V_h are nonlinear, and the relation between $\Delta R_p(t)$ and the activities of reactants, intermediates and products of the chemical reactions driving heteroepitaxial growth is nonlinear, the extraction of kinetic parameters from the measured time dependence of the PR signal generally requires numerical modeling. Combination of PRS with supplementing methods of optical real time process monitoring, such as RDS, SPA and LLS, is important for separating effects of bulk film growth, compositional changes in the SRL and roughening of the surface and buried interfaces. A key area of future research is the initial period of nucleation and coalescence of islands on the surface of the substrate.

Acknowledgements

Appendix A. Modeling of R_{p4}

For a four-layer stack, the complex reflectivity is given by

$$r_p = \frac{r_{12}[1 + r_{23}r_{34}e^{i2\beta_3}] + [r_{23} + r_{34}e^{i2\beta_3}]e^{i2\beta_2}}{1 + r_{23}r_{34}e^{i2\beta_3} + r_{12}[r_{23} + r_{34}e^{i2\beta_3}]e^{i2\beta_2}}, \tag{A.1}$$

with phase angles associated with layers 2 and 3

$$\beta_k = \frac{2\pi\delta_k}{\lambda}\sqrt{\varepsilon_k - \varepsilon_1 \sin^2 \varphi_1}, \quad k = 2, 3 \tag{A.2}$$

and Fresnell coefficients for the three interfaces 1–2, 2–3 and 3–4

$$r_{k,k+1} = \frac{\varepsilon_{k+1}\sqrt{\varepsilon_k - \varepsilon_1 \sin^2 \varphi_1} - \varepsilon_k\sqrt{\varepsilon_{k+1} - \varepsilon_1 \sin^2 \varphi_1}}{\varepsilon_{k+1}\sqrt{\varepsilon_k - \varepsilon_1 \sin^2 \varphi_1} + \varepsilon_k\sqrt{\varepsilon_{k+1} - \varepsilon_1 \sin^2 \varphi_1}}, \quad k = 1, 2, 3. \tag{A.3}$$

The dielectric function of the kth component of the four-layer stack is labeled ε_k. φ_1 is the angle of incidence in the ambient – chosen to be close to the pseudo-Brewster angle φ_{pB} for the substrate/vacuum interface. For the conditions of PCBE, the ambient dielectric function $\varepsilon_{11} = 1$. Since $\delta_2 \ll \lambda$, Eq. (1) can be linearized, i.e., the Maclaurin expansion of r_p

$$r_{p4} = r_{p4}|_{\beta_2 = 0} + \left(\frac{\partial r_{p4}}{\partial \beta_2}\bigg|_{\beta_2 = 0}\right)\beta_2 + \cdots \tag{A.4}$$

can be terminated in good approximation after the first order term in β_2. The reflectivity R_p is obtained by multiplication by the complex conjugate r_p^* of r_p, i.e.,

$$R_{p4} = r_{p4}r_{p4}^* = [\text{Re}(r_{p4})]^2 + [\text{Im}(r_{p4})]^2 \approx |r_{p4}|_{\beta_2=0}|^2 + \left|\beta_2\left(\frac{\partial r_{p4}}{\partial \beta_2}\Big|_{\beta_2=0}\right)\right|^2$$

$$+ 2\text{Re}\{r_{p4}|_{\beta_2=0}\}\text{Re}\left\{\beta_2\left(\frac{\partial r_{p4}}{\partial \beta_2}\Big|_{\beta_2=0}\right)\right\} + 2\,\text{Im}\{r_{p4}|_{\beta_2=0}\} + \text{Im}\left\{\beta_2\left(\frac{\partial r_{p4}}{\partial \beta_2}\Big|_{\beta_2=0}\right)\right\}. \tag{A.5}$$

From Eq. (A.1) follows

$$r_p|_{\beta_2=0} = \frac{r_{12} + r_{23} + (1 + r_{12}r_{23})r_{34}e^{i2\beta_3}}{1 + r_{12}r_{23} + (r_{12} + r_{23})r_{34}e^{i2\beta_3}} = \frac{(r_{12} + r_{23})/(1 + r_{12}r_{23}) + r_{34}e^{i2\beta_3}}{1 + [(r_{12} + r_{23})/(1 + r_{12}r_{23})]\,r_{34}e^{i2\beta_3}}. \tag{A.6}$$

Now, using Eq. (A.3) we obtain

$$r_{12} + r_{23} = \frac{2\varepsilon_2\varepsilon_3\sqrt{\varepsilon_1 - \varepsilon_1\sin^2\varphi_1}\,\sqrt{\varepsilon_2 - \varepsilon_1\sin^2\varphi_1} - 2\varepsilon_1\varepsilon_2\sqrt{\varepsilon_2 - \varepsilon_1\sin^2\varphi_1}\,\sqrt{\varepsilon_3 - \varepsilon_1\sin^2\varphi_1}}{(\varepsilon_2\sqrt{\varepsilon_1 - \varepsilon_1\sin^2\varphi_1} + \varepsilon_1\sqrt{\varepsilon_2 - \varepsilon_1\sin^2\varphi_1})(\varepsilon_3\sqrt{\varepsilon_2 - \varepsilon_1\sin^2\varphi_1} + \varepsilon_2\sqrt{\varepsilon_3 - \varepsilon_1\sin^2\varphi_1})} \tag{A.7}$$

$$1 + r_{12}r_{23} = \frac{2\varepsilon_2\varepsilon_3\sqrt{\varepsilon_1 - \varepsilon_1\sin^2\varphi_1}\,\sqrt{\varepsilon_2 - \varepsilon_1\sin^2\varphi_1} + 2\varepsilon_1\varepsilon_2\sqrt{\varepsilon_2 - \varepsilon_1\sin^2\varphi_1}\,\sqrt{\varepsilon_3 - \varepsilon_1\sin^2\varphi_1}}{(\varepsilon_2\sqrt{\varepsilon_1 - \varepsilon_1\sin^2\varphi_1} + \varepsilon_1\sqrt{\varepsilon_2 - \varepsilon_1\sin^2\varphi_1})(\varepsilon_3\sqrt{\varepsilon_2 - \varepsilon_1\sin^2\varphi_1} + \varepsilon_2\sqrt{\varepsilon_3 - \varepsilon_1\sin^2\varphi_1})} \tag{A.8}$$

Therefore,

$$\frac{r_{12} + r_{23}}{1 + r_{12}r_{23}} = \frac{\varepsilon_3\sqrt{\varepsilon_1 - \varepsilon_1\sin^2\varphi_1} - \varepsilon_1\sqrt{\varepsilon_3 - \varepsilon_1\sin^2\varphi_1}}{\varepsilon_3\sqrt{\varepsilon_1 - \varepsilon_1\sin^2\varphi_1} + \varepsilon_1\sqrt{\varepsilon_3 - \varepsilon_1\sin^2\varphi_1}} \equiv r_{13}. \tag{A.9}$$

Substituting the identity Eq. (A.9) into Eq. (A.6) yields

$$r_p|_{\beta_2=0} \equiv \frac{r_{13} + r_{34}e^{i2\beta_3}}{1 + r_{13}r_{34}e^{i2\beta_3}} \equiv r_{p3} \tag{A.10}$$

which is identical to the complex reflectivity r_{p3} for the three-layer stack: ambient/epilayer/substrate. Separating into the real and imaginary parts, i.e., $r_{kl} = r_{klr} + ir_{kli}$, $\beta_3 = \beta_{3r} + i\beta_{3i}$ and $e^{i\beta_{3r}} = \cos\beta_{3r} + i\sin\beta_{3r}$

$$r_p|_{\beta_2=0} = \frac{a_1 b_1 + a_2 b_2}{b_1^2 + b_2^2} + i\frac{a_2 b_1 - a_1 b_2}{b_1^2 + b_2^2}, \tag{A.11}$$

where

$$a_1 = r_{13r} + r_{34r}\cos(2\beta_{3r})e^{-2\beta_{3i}} - r_{34i}\sin(2\beta_{3r})e^{-2\beta_{3i}}, \tag{A.12}$$

$$a_2 = r_{13i} + r_{34i}\cos(2\beta_{3r})e^{-2\beta_{3i}} + r_{34r}\sin(2\beta_{3r})e^{-2\beta_{3i}}, \tag{A.13}$$

$$b_1 = 1 + [r_{13r}r_{34r} - r_{13i}r_{34i}]\cos(2\beta_{3r})e^{-2\beta_{3i}} - [r_{13r}r_{34i} + r_{13i}r_{34r}]\sin(2\beta_{3r})e^{-2\beta_{3i}}, \tag{A.14}$$

$$b_2 = [r_{13r}r_{34i} + r_{13i}r_{34r}]\cos(2\beta_{3r})e^{-2\beta_{3i}} + [r_{13r}r_{34r} - r_{13i}r_{34i}]\sin(2\beta_{3r})e^{-2\beta_{3i}}. \tag{A.15}$$

From Eq. (A.10) follows trivially

$$R_{p3} = r_{p3}r_{p3}^* = \frac{a_1^2 + a_2^2}{b_1^2 + b_2^2}. \tag{A.16}$$

The values of thickness $\delta_3(n)$ of the epilayer at which extrema exist in R_{p3} are obtained by setting the first derivative of Eq. (A.16) with respect to β_3 to zero. From Eq. (A.16) we get

$$\frac{\partial R_{p3}}{\partial \beta_3} = -\frac{4r_{13r}(r_{34r}\sin 2\beta_{3r} + r_{34i}\cos 2\beta_{3r})(1 - r_{13r}^2)(1 - |r_{34}|^2)}{[1 + r_{13r}^2|r_{34}|^2 + 2r_{13r}(r_{34r}\cos 2\beta_{3r} - r_{34i}\sin 2\beta_{3r})]^2}, \tag{A.17}$$

Hence, $\partial R_{p3}/\partial \beta_3 = 0$ when

$$r_{34r}\sin 2\beta_{3r} + r_{34i}\cos 2\beta_{3r} = 0 \tag{A.18}$$

or

$$\tan 2\beta_{3r} = -\frac{r_{34i}}{r_{34r}}, \tag{A.19}$$

which implies

$$\beta_{3r} = \frac{1}{2}\tan^{-1}\left(-\frac{r_{34i}}{r_{34r}}\right) + \frac{n\pi}{2}, \quad n = 0, 1, 2, \dots . \tag{A.20}$$

Using Eq. (A.2), extrema exist at

$$\delta_3(n) = \frac{(n + 2\gamma)\lambda}{4\sqrt{\varepsilon_3 - \varepsilon_1\sin\varphi_1}}, \tag{A.21}$$

where

$$\gamma = \frac{\tan^{-1}(-r_{34i}/r_{34r})}{2\pi} \tag{A.22}$$

represents a shift of the origin of the PR signal with regard to the first minimum in the evolution of the interference oscillations. From Eq. (A.21) follows Eq. (9) for the distance between maxima or minima in R_{p3}.

The last three terms in Eq. (A.5) represent the difference ΔR_{pl} between the linearized form $R_{p4\sim}$ of R_{p4} for the four-layer stack ambient–SRL–epilayer–substrate and the reflectance of a three-layer stack ambient–epilayer–substrate R_{p3}, i.e.,

$$\Delta R_{pl} = R_{p4\sim} - R_{p3} = \left|\beta_2\left(\frac{\partial r_p}{\partial \beta_2}\bigg|_{\beta_2=0}\right)\right|^2 + 2\mathrm{Re}\{r_p|_{\beta_2=0}\}\mathrm{Re}\left\{\beta_2\left(\frac{\partial r_p}{\partial \beta_2}\bigg|_{\beta_2=0}\right)\right\}$$

$$+ 2\,\mathrm{Im}\{r_p|_{\beta_2=0}\}\,\mathrm{Im}\left\{\beta_2\left(\frac{\partial r_p}{\partial \beta_2}\bigg|_{\beta_2=0}\right)\right\}. \tag{A.23}$$

ΔR_{pl} thus contains the essential information on the time dependence of R_{p4} in response to the changes in the composition and thickness of the SRL caused by the pulsed exposure to alternating fluxes of the source vapor molecules. Differentiation of Eq. (A.1) with regard to β_2 results

$$\frac{\partial r_p}{\partial \beta_2} = \mathrm{i}2\mathrm{e}^{\mathrm{i}2\beta_2}\frac{(1 - r_{12}^2)(r_{23} + r_{34}\mathrm{e}^{\mathrm{i}2\beta_3})(1 + r_{23}r_{34}\mathrm{e}^{\mathrm{i}2\beta_3})}{(1 + r_{23}r_{34}\mathrm{e}^{\mathrm{i}2\beta_3} + r_{12}[r_{23} + r_{34}\mathrm{e}^{\mathrm{i}2\beta_3}]\mathrm{e}^{-\mathrm{i}2\beta_2})^2} \tag{A.24}$$

so that

$$\left(\frac{\partial r_p}{\partial \beta_2}\bigg|_{\beta_2=0}\right)\beta_2 = \mathrm{i}2\beta_2\frac{(1 - r_{12}^2)(r_{23} + r_{34}\mathrm{e}^{\mathrm{i}2\beta_3})(1 + r_{23}r_{34}\mathrm{e}^{\mathrm{i}2\beta_3})}{(1 + r_{23}r_{34}\mathrm{e}^{\mathrm{i}2\beta_3} + r_{12}[r_{23} + r_{34}\mathrm{e}^{\mathrm{i}2\beta_3}])^2}. \tag{A.25}$$

Taking the input parameters given in the left column of Table 1 for the heteroepitaxial growth of GaP on Si under the conditions of PCBE results in the Fresnel coefficients given in the right-hand side column. They all are small compared to one. This property persists for an extended range of the real and imaginary parts of the dielectric function of the SRL, i.e., $8 \leqslant \varepsilon_{2r} \leqslant 25$ and $0 \leqslant \varepsilon_{2i} \leqslant 5$, corresponding to $r_{12r} < 0.145$, $r_{12i} < 0.125$, $r_{23r} < 0.203$ and $r_{23i} < 0.126$. Therefore, dropping products of Fresnell coefficients, the range of ε_2 Eq. (A.25) may be simplified further to

$$\left(\frac{\partial r_p}{\partial \beta_2}\Big|_{\beta_2=0}\right)\beta_2 \approx i2(r_{23} + r_{34}e^{i2\beta_3})\beta_2 = -2(a'_1\beta_{2i} + a'_2\beta_{2r}) + i2(a'_1\beta_{2r} - a'_2\beta_{2i}) \tag{A.26}$$

with

$$a'_1 = r_{23r} + r_{34r}\cos(2\beta_{3r})e^{-2\beta_{3i}} - r_{34i}\sin(2\beta_{3r})e^{-2\beta_{3i}}, \tag{A.27}$$

$$a'_2 = r_{23i} + r_{34i}\cos(2\beta_{3r})e^{-2\beta_{3i}} + r_{34r}\sin(2\beta_{3r})e^{-2\beta_{3i}}. \tag{A.28}$$

At the upper limit of the range of ε_2 this corresponds to an underestimation of $\beta_2(\partial r_p/\partial\beta_2|_{\beta_2=0})$ by $\sim 1\%$. Substitution of Eq. (A.26) into Eq. (A.23) results in the simplified approximation to the reflectance in the compact form of Eq. (8), where

$$A = -4(a'^2_1 + a'^2_2), \tag{A.29}$$

$$B = -4\left\{\frac{b_1}{b_1^2 + b_2^2}(a_1 a'_2 - a'_1 a_2) + \frac{b_2}{b_1^2 + b_2^2}(a_2 a'_2 + a_1 a'_1)\right\}, \tag{A.30}$$

$$C = -4\left\{\frac{b_1}{b_1^2 + b_2^2}(a_1 a'_1 + a_2 a'_2) - \frac{b_2}{b_1^2 + b_2^2}(a_1 a'_2 - a_2 a'_1)\right\}, \tag{A.31}$$

with $b_2 \ll b_1 \approx 1$ Eqs. (A.30) and (A.31) can be simplified to

$$B \approx -4(a_1 a'_2 - a'_1 a_2), \tag{A.32}$$

$$C \approx -4(a'_1 a_1 + a_2 a'_2), \tag{A.33}$$

We note that since

$$r_{23} = \frac{\varepsilon_3\sqrt{\varepsilon_2 - \varepsilon_1 \sin^2\varphi_1} - \varepsilon_2\sqrt{\varepsilon_3 - \varepsilon_1 \sin^2\varphi_1}}{\varepsilon_2\sqrt{\varepsilon_2 - \varepsilon_1 \sin^2\varphi_1} + \varepsilon_2\sqrt{\varepsilon_3 - \varepsilon_1 \sin^2\varphi_1}}, \tag{A.34}$$

A, B and C are functions of both ε_2 and ε_3.

Appendix B. Relation between the reflectance and the composition of the SRL

For the interpretation of the time-dependence of R_p in terms of the chemical kinetics in the SRL that drives epitaxial growth in steady-state ε_2 must be linked to the composition of the SRL. Such a linkage is given by the Sellmeier equation:

$$\varepsilon(\omega) = 1 - \frac{4\pi Nq^2}{mV}\sum_{\Psi_k \to \Psi_j}\left\{\frac{f_{kj}}{\omega^2 - \omega_{kj}^2 + i\Gamma_{kj}\omega}\right\} \tag{B.1}$$

that describes the dielectric function of a pure substance in terms of the electronic transitions from filled states Ψ_k to empty states Ψ_j allowed by symmetry for the molecules of this particular substance. In Eq. (B.1) ω is the frequency at which ε is evaluated, N is the number of molecules in volume V and $-q$ and m are the

electronic charge and mass. $E_{kj} = h\omega_{kj}$ is the energy of the transition, Γ_{kj} is the associated broadening parameter, and $f_{kj} = (2m|\xi \mu_{kj}|^2 E_{kj})/q^2 h^2$ is the oscillator strength of the electronic transition $\Psi_k \rightarrow \Psi_j$ expressed in terms of the component of the polarization vector ξ of the exciting electromagnetic wave along matrix elements of the electric dipole operator $\mu_{kj} = -q\langle \Psi_k|r|\Psi_j\rangle$.

The dielectric function of the SRL is obtained by summing over the contributions of all its constituent – identified by labels $h = 1, 2, \ldots$, i.e.,

$$\varepsilon_2(\omega) = 1 - \frac{4\pi q^2 N_A}{m} \sum_h c_h \sum_{\Psi_{kh} \rightarrow \Psi_{jh}} \left\{ \frac{f_{kjh}}{\omega^2 - \omega_{kjh}^2 + i\Gamma_{kjh}\omega} \right\}. \tag{B.2}$$

This is equivalent to Eq. (10), where the second sum in Eq. (B.2) has been abbreviated as $F_h(\omega)$.

In particular, for the condition of III–V heteroepitaxy frequently $\varepsilon_{2r} \gg \varepsilon_1 \sin^2 \varphi_1$ and $\varepsilon_{2r} \gg \varepsilon_{2i}$, so that at low surface coverage where the SRL approaches the behavior of an ideal mixture

$$\sqrt{\varepsilon_{2r} - \varepsilon_1 \sin^2 \varphi_1 + i\varepsilon_{2i}} \approx \sqrt{\varepsilon_{2r} + i\varepsilon_{2i}} \approx \sqrt{\varepsilon_{2r}} + i\frac{\varepsilon_{2i}}{2\sqrt{\varepsilon_{2r}}}. \tag{B.3}$$

Then ΔR_p may be modeled using the expression

$$\Delta R_{ps}(t) \approx A \frac{4\pi^2 \delta_2(t)^2}{\lambda^2} \{[\text{Re}(\sqrt{\varepsilon_2})]^2 + [\text{Im}(\sqrt{\varepsilon_2})]^2\} + B \frac{2\pi\delta_2(t)}{\lambda} \sqrt{\varepsilon_{2r}} + C \frac{2\pi\delta_2(t)}{\lambda} \frac{\varepsilon_{2i}}{2\sqrt{\varepsilon_{2r}}}$$

$$= A \frac{4\pi^2 \delta_2(t)^2}{\lambda^2} \frac{\varepsilon_{2r}^2 + \varepsilon_{2i}^2}{\varepsilon_{2r}} + B \frac{2\pi\delta_2(t)}{\lambda} \sqrt{\varepsilon_{2r}} + C \frac{\pi\delta_2(t)}{\lambda} \frac{\varepsilon_{2i}}{\sqrt{\varepsilon_{2r}}}. \tag{B.4}$$

Separating Eq. (B.2) into real and imaginary parts, we get

$$\varepsilon_{2r}(\omega) = 1 - \frac{4\pi q^2 N_A}{m} \sum_h c_h F_{hr}(\omega), \tag{B.5}$$

and

$$\varepsilon_{2ri}(\omega) = \frac{4\pi q^2 N_A}{m} \sum_h c_h F_{hi}(\omega), \tag{B.6}$$

with functions

$$F_{hr}(\omega) = \sum_{\Psi_{kh} \rightarrow \Psi_{jh}} \left\{ \frac{[\omega^2 - \omega_{kjh}^2] f_{kjh}}{[\omega^2 - \omega_{kjh}^2]^2 + \Gamma_{kjh}^2 \omega^2} \right\}, \tag{B.7}$$

$$F_{hi}(\omega) = \sum_{\Psi_{kh} \rightarrow \Psi_{jh}} \left\{ \frac{\Gamma_{kjh}\omega f_{kjh}}{[\omega^2 - \omega_{kjh}^2]^2 + \Gamma_{kjh}^2 \omega^2} \right\}. \tag{B.8}$$

Thus, at low coverage, $\Delta R_{ps}(t)$ is represented by Eq. (12). Under conditions of high flux at low processing temperature, where the SRL behaves like a nonideal condensed phase, a realistic representation of vapor deposition and etching processes must account for modifications of both its dielectric function and the rate constants of the surface chemical reactions by the intermolecular interactions.

References

[1] N. Dietz, K.J. Bachmann, MRS Bull. 20 (1995) 49.
[2] U. Rossow, N. Dietz, K.J. Bachmann, D.E. Aspnes. J. Vac. Sci. Technol. B 14 (1996) 3040.

[3] K.J. Bachmann, U. Rossow, N. Dietz, Mater. Sci. Eng. B 37 (1995) 472.
[4] N. Dietz, K.J. Bachmann, Vacuum 47 (1996) 133.
[5] K.J. Bachmann, U. Rossow, N. Sukidi, H. Castleberry, N. Dietz, J. Vac. Sci. Technol. B 14 (1996) 3019.
[6] S.H. Li, C.A. Larsen, G.B. Stringfellow, J. Electron. Mater. 8 (1989) 457.
[7] W. Richter, P. Kurpas, R. Lückerath, M. Motzkus, M. Washbüsch, J. Crystal Growth 107 (1991) 13.
[8] G.H. Fan, R.D. Hoare, M.E. Pemble, I.M. Povey, A.G. Taylor, J.O. Williams, J. Crystal Growth 124 (1992) 49.
[9] P.E. Lee, T.R. Omstead, D.R. McKenna, K.F. Jensen, J. Crystal Growth 85 (1987) 165.
[10] T. Martin, C.R. Whitehouse, J. Crystal Growth 105 (1990) 199.
[11] N. Kobayashi, T. Makimoto, Y. Yamaguchi, Y. Horikoshi, J. Crystal Growth 107 (1991) 62.
[12] A. Robertson Jr., T.H. Chiu, W.T. Tsang, J. Cunningham, J. Appl. Phys. 92 (1988) 877.
[13] J.T. Kelliher, A.E. Miller, N. Dietz, S. Habermehl, Y.L. Chen, Z. Lu, G. Lucovsky, K.J. Bachmann, Appl. Surf. Sci. 86 (1995) 453.
[14] K.J. Bachmann, C. Höpfner, N. Sukidi, A.E. Miller, C. Harris, D.E. Aspnes, N. Dietz, H.T. Tran, S. Beeler, K. Ito, H.T. Banks, U. Rossow, Appl. Surf. Sci. 112 (1997) 38.
[15] G. Bauer, W. Richter, Optical Characterization of Epitaxial Semiconductors, Springer, Berlin, 1996.
[16] D.E. Aspnes, J. Vac. Sci. Technol. B 3 (1985) 1498.
[17] N. Kobayashi, Y. Horikoshi, Jpn. J. Appl. Phys. 30 (1991) L1443.
[18] K. Hingerl, D.E. Aspnes, I. Kamiya, L.T. Florez, Appl. Phys. Lett. 63 (1993) 885.
[19] K. Ploska, J.-Th. Zettler, W. Richter, J. Jönsson, F. Reinhardt, J. Rumberg, M. Pristovsek, M. Zorn, D. Westwood, R.H. Williams, J. Crystal Growth 145 (1994) 44.
[20] M. Zorn, J. Jönsson, A. Krost, W. Richter, J.-Th. Zettler, K. Ploska, F. Reinhardt, J. Crystal Growth 145 (1994) 53.
[21] P. Kurpas, J. Jönsson, W. Richter, D. Gutsche, M. Pristovsek, M. Zorn, J. Crystal Growth 145 (1994) 38.
[22] K.J. Bachmann, G. Martinelli-Kepler, Proc. SPIE 3123 (1997), submitted.
[23] N. Dietz, N. Sukidi, C. Harris, K.J. Bachmann, J. Vac. Sci. Technol. (1997), to appear.
[24] K.J. Laidler, Chemical Kinetics, Harper & Row, New York, 1987, p. 188.